Acta Crystallographica Section B
Structural Science
ISSN 0108-7681

Crystal structure and local order in $Co_6Al_{11-x}Si_{6+x}$

Klaus W. Richter,[a]* Yurii Prots,[b] Horst Borrmann,[b] Reiner Ramlau[b] and Yuri Grin[b]

[a]Department of Inorganic Chemistry/Materials Chemistry, University of Vienna, Währinger Strasse 42, 1090 Wien, Austria, and [b]Max-Planck-Institut für Chemische Physik fester Stoffe, Nöthnitzer Strasse 40, 01187 Dresden, Germany

Correspondence e-mail: klaus.richter@univie.ac.at

Received 8 February 2007
Accepted 18 June 2007

The ternary compound $Co_6Al_{11-x}Si_{6+x}$ (ε phase) was prepared from the elements by arc melting and subsequent heat treatment, and then characterized by single-crystal X-ray diffraction (XRD), electron-probe microanalysis (EPMA), differential thermal analysis (DTA) and transmission electron microscopy (TEM). This new structure type consists of planar layers with the composition $[Co_6Al_{10}Si_4]$, which are penetrated by perpendicular (Si—Si—Al) chains. While the layers are well described by an orthorhombic model (space group *Pnma*, Pearson symbol *oP*46), the chains exhibit doubled periodicity, thus yielding a superstructure. Two alternative ordering models (space group $Cmc2_1$, *oC*184, and space group $P2_1/c$, *mP*92) are presented and discussed based on XRD and TEM results. The (Si—Si—Al) chains are located in pentagonal antiprismatic 'channels' which reveal the similarity of the $Co_6Al_{11-x}Si_{6+x}$ structure to Al-rich transition-metal compounds such as Co_4Al_{13}, Co_2Al_5, Fe_4Al_{13}, V_7Al_{45}, V_4Al_{23} and VAl_{10}, which also exhibit this type of pentagonal 'channels' in their crystal structures. The phase shows only a very small homogeneity range.

1. Introduction

Transition-metal compounds containing aluminium and silicon show a rich and interesting chemistry, ranging from solid-solution phases with extended substitution among the main group elements to ternary compounds adopting complex structures with a very small homogeneity range and distinct lattice sites occupied by aluminium or silicon, respectively. During a recent investigation of the Ni–Al–Si system, we isolated a new compound with a very small homogeneity range, $Ni_{16}AlSi_9$ (Pearson symbol *oC*104, space group *Cmcm*, own structure type; Richter, Chandrasekaran & Ipser, 2004), in which aluminium partially enters only one of the four silicon positions and causes local symmetry breaking in the structure. At higher temperatures the respective composition area is dominated by extended solid-solution phases such as $Ni_{13\pm x}Si_{9-y}Al_y$ (*hP*66, $P3_121$, structure type $Ga_3Ge_6Ni_{13}$; Richter, 2002) or the solid solution of Al in δ-Ni_2Si (*oP*12, *Pnma*, structure type Co_2Si; Richter, Prots & Grin, 2004), both showing mixed site occupation of Al and Si.

In the Co–Al–Si system the Al-rich part turns out to be the most complex region of the ternary phase diagram (Richter & Tordesillas Gutiérrez, 2005). The binary Co–Al system at high aluminium content (> 70 at.% Al) contains a variety of phases (Gödecke & Ellner, 1996; Grushko *et al.*, 1996), including the compounds Co_2Al_9 (*mP*22, $P2_1/c$, own structure type; Douglas, 1950; Boström *et al.*, 2005), three different modifications of Co_4Al_{13} (Grin *et al.*, 1994*a*,*b*; Burkhardt *et al.*, 1996), a deca-

Table 1
Crystallographic data for $Co_6Al_{11-x}Si_{6+x}$.

Composition	$Co_6Al_{11-x}Si_{6+x}$		
Crystal size (mm)	0.030 × 0.035 × 0.140		
Calc. density (g cm^{-3})	4.33		
Absorption coefficient (Mo $K\alpha$), μ (mm^{-1})	9.34		
Diffractometer	Rigaku AFC7		
Detector	Mercury CCD		
Scans, step (°)	φ, ω, 0.6		
Wavelength (Å)	Mo $K\alpha$, 0.71073		
2θ range up to (°)	64		
N (images)	500		
Space group	*Pnma*	*Cmc*2$_1$	*P*2$_1$/*c*
Formula units/cell, Z	2	8	4
Unit-cell parameters†			
a (Å)	21.3536 (9)	8.0839 (3)	8.0839 (3)
b (Å)	4.0420 (3)	14.5445 (6)	21.3536 (9)
c (Å)	7.2723 (6)	21.3536 (9)	8.3200 (3)
β (°)	–	–	119.07 (1)
V (Å^3)	627.7 (1)	2510.7 (3)	1255.3 (2)
N(*hkl*)	7620	14 089	14 161
Ranges for h, k, l	$-31 \le h \le 31$	$-12 \le h \le 7$	$-12 \le h \le 7$
	$-6 \le k \le 3$	$-21 \le k \le 19$	$-31 \le k \le 31$
	$-9 \le l \le 10$	$-31 \le l \le 31$	$-12 \le l \le 11$
N(*hkl*) unique	1210	–‡	–‡
N(*hkl*) observed	1201	13 424	13 502
Refined parameters	77	231	210
R(F)	0.027	0.037	0.029
Maximum residual density peak (e Å^{-3})	1.64	2.34	2.21

† X-ray powder diffaction data for the sample composition $Co_{26}Al_{46}Si_{28}$. ‡ Not merged because of applied twinning approach.

gonal quasicrystalline phase between Co_4Al_{11} and Co_3Al_{10} (Ma & Kuo, 1992), its monoclinic approximant $CoAl_3$ (Li & Hiraga, 1998), and Co_2Al_5 (*hP*28, *P*6$_3$/*mmc*, own structure type; Burkhardt *et al.*, 1998). All Al-rich binary phases show pentagonal prismatic atomic arrangements and may be regarded as closely related to quasicrystals (Grin *et al.*, 1994*b*). This complex structural chemistry is continued in the Al-rich part of the ternary Co–Al–Si system. In an early phase-diagram investigation (Herman, 1981) three ternary phases designated γ, δ and ε were found in the Al-rich part, but no structural details were given. In our own studies, five ternary compounds with new structure types were prepared in this part of the Co–Al–Si system. The crystal structure of the χ phase, $Co_4Al_{7+x}Si_{2-x}$ (*mC*26, *C*2/*m*), as well as the complex crystal structures of the γ phase, $Co_{19-x}Al_{43+y}Si_{12-y}$ (*mC*296+, *C*2/*c*), and the φ phase, $Co_{10+x}Al_{23-x}Si_{9-2x}$ (*oP*168, *Pnma*), were recently reported (Richter *et al.*, 2005; Richter & Prots, 2006*a*,*b*). Along with the crystal structure determination of $Co_4Al_{7+x}Si_{2-x}$, chemical bonding was analyzed based on quantum chemical calculations (electron localization function, ELF). The δ phase with approximate composition $Co_{32}Al_{45}Si_{23}$ (*mC**) is incommensurately modulated and its structure has not been characterized up to now (Richter *et al.*, 2005). In this paper we report on the synthesis and crystal structure of the ε phase, $Co_6Al_{11-x}Si_{6+x}$, which was found to crystallize in a narrow composition range with very limited Al/Si substitution at the respective lattice sites.

2. Experimental

Samples were prepared from an aluminium rod (99.999%, Alfa AESAR), a silicon rod (99.9999%, Dow Corning) and cobalt pieces (99.9+%, Alfa AESAR). Stoichiometric amounts of the elements were weighed to an accuracy of 0.05 mg and then arc-melted on a water-cooled copper plate under an argon atmosphere using zirconium as a getter material. The obtained droplets with a total mass of approximately 1 g each were re-melted one or two times for homogenization and then weighed back in order to check for possible mass loss, which was found to be negligible (less than 1 mg) with respect to the final composition. The reguli were placed in alumina crucibles, which were sealed in evacuated quartz glass ampoules. The samples were heated to 1323 K within a day, cooled slowly to 1073 K at a rate of 5 K h^{-1} and then annealed at 1073 K for 4 weeks. After quenching in water, the samples were investigated using X-ray diffraction (XRD), electron-probe microanalysis (EPMA), scanning electron microscopy (SEM), metallographic analysis, differential thermal analysis (DTA) and transmission electron microscopy (TEM).

The phase identification was performed by X-ray powder diffraction, using a Guinier camera (Huber G670) equipped with an image-plate detection system and employing Co $K\alpha_1$ radiation (λ = 1.788965 Å). Precise lattice parameter determination was performed using LaB_6 (a = 4.15692 Å) as an internal standard.

Polished pieces of the annealed samples were investigated by optical microscopy and the composition of the identified phases was analyzed by EPMA. These measurements were carried out on a Cameca SX 100 microprobe using wavelength-dispersive X-ray spectroscopy (WDXS) employing elemental aluminium, silicon and cobalt as standard materials. The measurements were carried out at 15 kV using a beam current of 20 nA. A conventional ZAF matrix correction (Z: atomic number, A: absorption, F: fluorescence) was applied to derive the final composition. The composition of the single crystal was analyzed with energy-dispersive X-ray spectroscopy (EDXS) in a Philips XL30 scanning electron microscope.

The single-crystal X-ray investigation was carried out on a Rigaku AFC7 diffractometer equipped with a Mercury CCD detector. For more details see Table 1. Crystallographic calculations were performed with the program packages *SHELXL*97 (Sheldrick, 1997) and *WinCSD* (Akselrud *et al.*, 1993).

The decomposition temperature of the $Co_6Al_{11-x}Si_{6+x}$ phase was determined with a high-temperature DTA instrument (Netzsch, S404) at a heating rate of 5 K min^{-1} using open alumina crucibles and applying a permanent argon flow. Samples of about 150 mg were used for the experiments. The Pt–PtRh thermocouples of the instrument were calibrated at the melting points of pure Al, Au and Ni.

For TEM investigation the powder-like starting material was further crushed in an agate mortar, dispersed in *n*-butanol and spread over a holey carbon film. The FEI Tecnai F30 G^2

Table 2
Composition of the ε phase in various phase fields determined by EPMA.

Nominal sample composition	Phase field	Composition of the ε phase
$Co_{24}Al_{52}Si_{24}$	$[Co_6Al_{11-x}Si_{6+x} + Co_{10+x}Al_{23}Si_{9-2x}]$	$Co_{26.4\,(1)}Al_{45.5\,(1)}Si_{28.1\,(1)}$
$Co_{26}Al_{54}Si_{20}$	$[Co_6Al_{11-x}Si_{6+x} + Co_{19-x}Al_{43+y}Si_{12-y}]$	$Co_{26.6\,(2)}Al_{45.8\,(2)}Si_{27.6\,(2)}$
$Co_{28}Al_{48}Si_{24}$	$[Co_6Al_{11-x}Si_{6+x} + Co_{19-x}Al_{43+y}Si_{12-y} + Co_{32.5}Al_{43}Si_{24.5}]$	$Co_{26.5\,(1)}Al_{45.8\,(1)}Si_{27.7\,(1)}$
$Co_{28}Al_{44}Si_{28}$	$[Co_6Al_{11-x}Si_{6+x} + Co_{32.5}Al_{43}Si_{24.5} + Co_2Al_{1+x}Si_{2-x}]$	$Co_{26.5\,(1)}Al_{45.5\,(1)}Si_{28.0\,(1)}$
$Co_{30}Al_{38}Si_{32}$	$[Co_6Al_{11-x}Si_{6+x} + Co_2Al_{1+x}Si_{2-x} + Co_3Al_{3-x}Si_{4+x}]$	$Co_{26.4\,(2)}Al_{45.3\,(2)}Si_{28.3\,(2)}$
$Co_{26}Al_{42}Si_{32}$	$[Co_6Al_{11-x}Si_{6+x} + Co_2Al_{1+x}Si_{2-x} + Si]$	$Co_{26.2\,(1)}Al_{44.4\,(1)}Si_{29.4\,(1)}$
$Co_{26}Al_{48}Si_{26}$	$[Co_6Al_{11-x}Si_{6+x} + Co_{32}Al_{45}Si_{23}]$	$Co_{26.3\,(2)}Al_{46.6\,(2)}Si_{27.1\,(2)}$

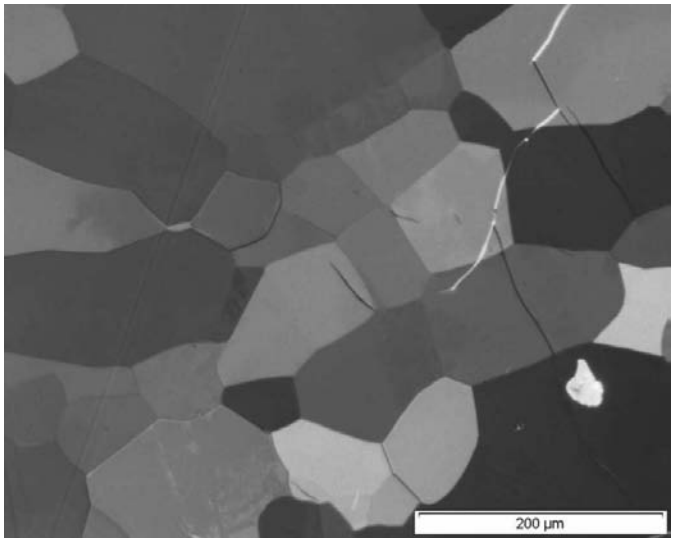

Figure 1
Microstructure of the sample with the nominal composition $Co_{26}Al_{46}Si_{28}$ annealed for 4 weeks at 1073 K (polarized light) showing large grains of $Co_6Al_{11-x}Si_{6+x}$. No signs for twinning were observed. The φ phase ($Co_{10+x}Al_{23-x}Si_{9-2x}$) is not visible in this area.

electron microscope with Supertwin lens was operated at 300 kV (spherical aberration constant $C_S = 1.2$ mm, point resolution: 0.2 nm). Electron diffraction (ED) patterns were registered on photographic film or with a Gatan US1000 CCD camera. It turned out that the compound readily decomposes under electron irradiation, which made the investigation rather difficult. Kinematical ED diffraction patterns were simulated with the *EMS* program package (Ecole Polytecnique Fédérale de Lausanne) or the *Ideal-Microscope* program (EMLAB software).

3. Results and discussion

The title compound was observed during a systematic investigation of the composition range adjacent to the binary Co–Al system between 20 and 36 at. % Co and between 4 and 32 at. % Si, respectively. A fine grid of approximately 50 samples was prepared according to the procedure described in the previous section and all samples were initially investigated by powder XRD and metallography. The composition area of the ε phase was determined by EPMA (Table 2). Experimental results show a narrow homogeneity range, $Co_{26.4}Al_{44.4–46.6}Si_{29.2–27.0}$. The orthorhombic lattice parameters derived from Guinier powder patterns (for the structural model in the space group $Cmc2_1$) are $a = 8.0778$ (3), $b = 14.5122$ (5), $c = 21.3500$ (6) Å for the silicon-rich composition (sample $Co_{26}Al_{42}Si_{32}$) and $a = 8.0852$ (4), $b = 14.5556$ (7), $c = 21.358$ (1) Å for the silicon-poor side (sample $Co_{26}Al_{48}Si_{26}$). This minor variation of lattice parameters is consistent with the very small composition area determined by EPMA (Table 2).

The microstructure of a sample with nominal composition $Co_{26}Al_{46}Si_{28}$ is shown in Fig. 1. It consists of large grains of the ε phase showing strong polarization effects. A few isolated small grains of the neighboring φ phase $Co_{10+x}Al_{23-x}Si_{9-2x}$ (Richter & Prots, 2006*b*) were also identified in the sample.

The DTA investigation of this sample showed a strong invariant effect at 1184 K (value determined from the heating curve), which may be interpreted as the peritectic decomposition of $Co_6Al_{11-x}Si_{6+x}$; the liquidus point was found at 1371 K (value determined from the cooling curve). Additional DTA experiments in samples containing $Co_6Al_{11-x}Si_{6+x}$ in equilibrium with neighboring phases confirmed the decomposition temperature at 1184 ± 2 K.

Suitable single crystals for diffraction data collection were mechanically separated from an annealed sample with nominal composition $Co_{26}Al_{46}Si_{28}$. Oscillation images around the crystallographic axes were recorded on the Rigaku AFC7 diffractometer with a CCD detector, and clearly indicated a primitive orthorhombic subcell with $a = 21.3536$ (9), $b = 4.0420$ (3) and $c = 7.2723$ (3) Å. However, weak superstructure reflections required the doubling of unit-cell parameters b and c. To obtain accurate intensities of strong and weak reflections two measurements with long and short exposure times were performed. The two data sets were scaled and combined using the program *XPREP* (Bruker Analytical X-ray Instruments Inc., 1997).

In the first step of the structure determination we solved and refined the structure in a primitive orthorhombic subcell (*oP*46, *Pnma*), ignoring all superstructure reflections. The structural model ($R_F = 0.025$) is described by only 12 independent atomic sites.[1] A detailed inspection of interatomic distances subsequently revealed two distinctly different sets of main-group element positions (which were preliminarily refined as Al positions): the first set of atoms (Si1–Si3) shows contacts to Co at around 2.27 Å resembling short Co—Si interactions, but are definitely too small for Co—Al contacts [covalent radii: r(Co) = 1.16, r(Al) = 1.25,

[1] Supplementary data for this paper are available from the IUCr electronic archives (Reference: SN5051). Services for accessing these data are described at the back of the journal.

Table 3
Selected interatomic distances (Å) for $Co_6Al_{11-x}Si_{6+x}$ (space group *Pnma*).

Co1—1Si1	2.235 (2)	Al3—2Co2	2.442 (1)
Co1—1Si2	2.258 (2)	Al3—1Co2	2.487 (2)
Co1—2Si2	2.4175 (8)	Al3—2Si3†	2.561 (3)
Co1—2Al5	2.482 (1)	Al3—1Al6†	2.634 (5)
Co1—1Al2	2.600 (2)	Al3—2Si1	2.648 (2)
Co1—1Al5	2.691 (2)	Al3—2Al4	2.701 (2)
Co1—2Co1	2.7111 (6)	Al3—1Al4	2.784 (2)
Co2—1Si1	2.277 (2)	Al4—2Co2	2.502 (1)
Co2—2Si3†	2.301 (2)	Al4—2Si3†	2.571 (3)
Co2—2Al3	2.442 (1)	Al4—1Co3	2.683 (2)
Co2—1Al3	2.487 (2)	Al4—2Al3	2.701 (2)
Co2—2Al4	2.502 (1)	Al4—1Co2	2.707 (2)
Co2—1Al2	2.595 (2)	Al4—2Al2	2.734 (2)
Co2—1Al4	2.707 (2)	Al4—1Al3	2.784 (2)
Co3—2Si3†	2.285 (2)	Al5—2Co1	2.482 (1)
Co3—1Si2	2.288 (2)	Al5—1Co3	2.530 (2)
Co3—2Al1	2.428 (1)	Al5—2Si3†	2.684 (3)
Co3—2Al2	2.529 (1)	Al5—1Co1	2.691 (2)
Co3—1Al5	2.530 (2)	Al5—1Si2	2.716 (2)
Co3—1Al1	2.626 (2)	Al5—2Al1	2.759 (2)
Co3—1Al4	2.683 (2)	Al5—2Si1	2.802 (2)
Al1—2Co3	2.428 (1)	Si1—1Co1	2.235 (2)
Al1—1Si2	2.569 (2)	Si1—1Co2	2.277 (2)
Al1—1Co3	2.626 (2)	Si1—1Al6†	2.390 (4)
Al1—2Al1	2.659 (2)	Si1—2Si3†	2.527 (3)
Al1—1Al2	2.739 (2)	Si1—1Al2	2.587 (2)
Al1—2Al5	2.759 (2)	Si1—2Al3	2.648 (2)
Al1—1Al6†	2.836 (5)	Si1—2Al5	2.802 (2)
Al2—2Co3	2.529 (1)	Si2—1Co1	2.258 (2)
Al2—1Si1	2.587 (2)	Si2—1Co3	2.288 (2)
Al2—1Co2	2.595 (2)	Si2—2Co1	2.4175 (8)
Al2—1Co1	2.600 (2)	Si2—1Al1	2.569 (2)
Al2—1Al6†	2.625 (5)	Si2—2Al2	2.629 (1)
Al2—2Si2	2.629 (1)	Si2—1Al5	2.716 (2)
Al2—2Al4	2.734 (2)		
Al2—1Al1	2.739 (2)		

† Occupancy 0.50. For distances involving the half-occupied positions Al6 and Si3, see Table 4.

r(Si) = 1.17 Å; Emsley, 1994]. The second group of atoms (Al1–Al6) shows Co—Al distances at around 2.45 Å (Table 3). Considering distances to Co, it was thus possible to distinguish Al from Si positions in an unambiguous way. The chemical composition $Co_6Al_{11}Si_6$ ($Co_{26.1}Al_{47.8}Si_{26.1}$) derived from crystal structure refinement corresponds very well with the composition derived from EPMA and the ratio of starting components (Table 2). A small deviation to the Si-rich side of $Co_6Al_{11}Si_6$ was observed. EDXS analysis of the crystal used in structure analysis (only semi-quantitative owing to the lack of plane surfaces of the crystal) yielded the composition $Co_{27\,(2)}Al_{44\,(2)}Si_{29\,(2)}$ (mean value of 4 independent measurements), which is also in good agreement with the overall composition of the sample. This fact as well as the very limited composition range is a strong support for distinct Al and Si positions in this compound as it has been derived based on interatomic distance analysis.

The atomic positions with full occupancy are all situated within the mirror planes at $y = \frac{1}{4}$ and $y = \frac{3}{4}$ forming layers with an overall stoichiometry of $[Co_6Al_{10}Si_4]$. The atomic arrangement within the layers is shown in Fig. 2. According to space-group symmetry, adjacent layers situated at $y = \frac{1}{4}$ and $y = \frac{3}{4}$ show inverted orientation. The Si3 position is situated at a general 8(*d*) site displaced from the layers. Together with the Al6 position with 50% occupation, Si3 forms (Si—Si—Al) chains perpendicular to the layers. The penetration points are arranged in a zigzag motif, as shown by dotted lines. There are two different kinds of penetration points in every layer: one is located in a larger void and contains Al6, while the other one has Si3 atoms above/below the layer.

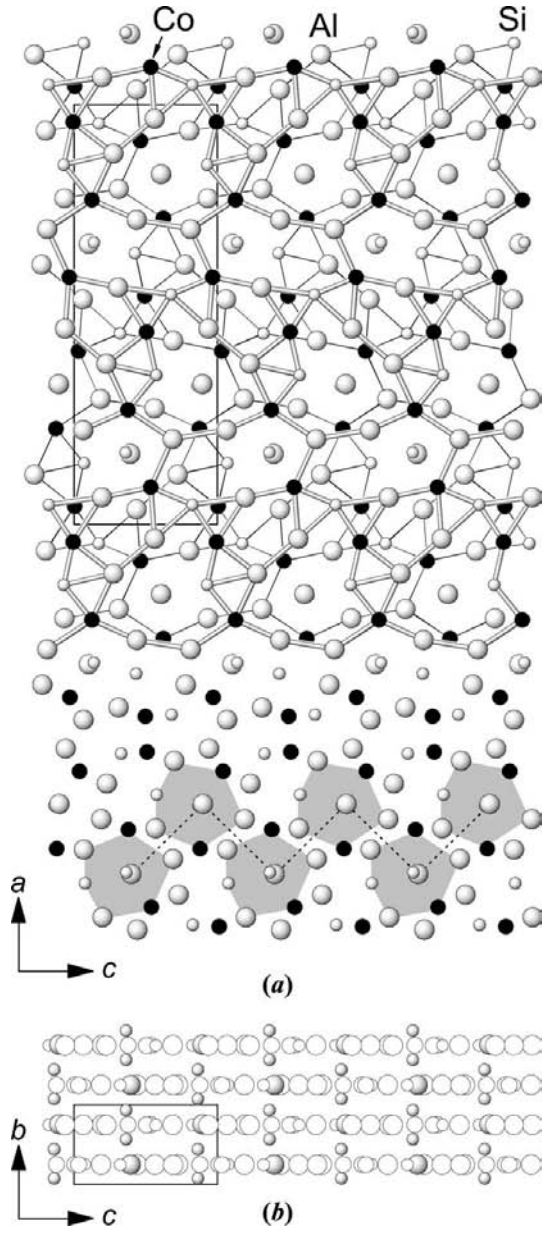

Figure 2
Crystal structure of $Co_6Al_{11-x}Si_{6+x}$ (*Pnma* substructure model). (*a*) Planar layers perpendicular to the *b* axis. Adjacent layers shown by sticks of different thickness reveal an inverted atomic arrangement. All interatomic distances up to 3.0 Å are shown within each layer. One set of the pentagonal-like channels with the interpenetrating perpendicular (Si—Si—Al) chains are marked in gray. Atoms within the chains have a 50% occupation in the *Pnma* model. The zigzag motif of adjacent chains is marked by dotted lines. (*b*) Projection of the structure along [100]. For a clearer visualization of the (Si—Si—Al) chains the atoms of the layers are represented as white circles.

Table 4
Selected interatomic distances (Å) for the atomic sites located in the pentagonal channels for the different structural models of $Co_6Al_{11-x}Si_{6+x}$.

'*Pnma*' model			
Al6†—2Si3†	1.309 (3)	Si3†—1Co3	2.285 (2)
Al6†—1Si1	2.390 (4)	Si3†—1Co2	2.301 (2)
Al6†—1Al2	2.625 (5)	Si3†—1Si1	2.527 (3)
Al6†—1Al3	2.634 (5)	Si3†—1Al3	2.561 (3)
Al6†—2Si3†	2.769 (3)	Si3†—1Si3†	2.569 (4)
Al6†—2Co3	2.815 (3)	Si3†—1Al4	2.571 (3)
Si3†—1Al6†	1.309 (3)	Si3†—1Al5	2.684 (3)
Si3†—1Si3†	1.473 (4)	Si3†—1Al6†	2.769 (3)
'$Cmc2_1$' model			
Al6*b*—1Si1*b*	2.451 (2)	Si3*a*†—1Si3*b*†	2.658 (4)
Al6*b*—1Al2*b*	2.753 (2)	Si3*a*†—1Al6*c*†	2.789 (4)
Al6*b*—2Co3*c*	2.772 (1)	Si3b†—1Al6*c*†	0.989 (4)
Al6*b*—2Si3*c*	2.7771 (9)	Si3*b*†—1Si3*b*†	1.697 (4)
Al6*b*—1Al3*b*	2.786 (2)	Si3*b*†—1Co3*a*	2.289 (3)
Al6*b*—1Al1*b*	2.894 (3)	Si3*b*†—1Co2*b*	2.297 (3)
Al6*c*†—1Si3*b*†	0.989 (4)	Si3*b*†—1Si1*c*	2.538 (3)
Al6*c*†—1Si3*a*†	1.725 (4)	Si3*b*†—1Al3*b*	2.545 (3)
Al6*c*†—1Si1*c*	2.418 (3)	Si3*b*†—1Al4*a*	2.577 (3)
Al6*c*†—1Al2*c*	2.618 (3)	Si3*b*†—1Si3*a*†	2.658 (3)
Al6*c*†—1Al3*c*	2.622 (4)	Si3*b*†—1Al6*c*†	2.671 (4)
Al6*c*†—1Co3*a*	2.670 (4)	Si3*b*†—1Al5*b*	2.706 (3)
Al6*c*†—1Si3*b*†	2.671 (4)	Si3*c*—1Co3*c*	2.294 (1)
Al6*c*†—1Si3*a*†	2.789 (4)	Si3*c*—1Co2*c*	2.325 (1)
Si3*a*†—1Si3*a*†	1.078 (3)	Si3*c*—1Si1*a*	2.482 (1)
Si3*a*†—1Al6*c*†	1.725 (4)	Si3*c*—1Si3*c*	2.549 (1)
Si3*a*†—1Co2*a*	2.282 (3)	Si3*c*—1Al4*c*	2.580 (1)
Si3*a*†—1Co3*b*	2.292 (3)	Si3*c*—1Al3*c*	2.580 (1)
Si3*a*†—1Si1*c*	2.526 (3)	Si3*c*—1Al5*c*	2.709 (2)
Si3*a*†—1Al3*a*	2.552 (3)	Si3*c*—1Al6*b*	2.7771 (9)
Si3*a*†—1Al4*b*	2.594 (3)	Si3*c*—1Al3*a*	2.840 (2)
Si3*a*†—1Al5*a*	2.639 (3)		
'$P2_1/c$' model			
Al6*a*—1Si1*b*	2.440 (1)	Si3*a*—1Al5*a*	2.684 (1)
Al6*a*—1Al2*b*	2.702 (1)	Si3*a*—1Al6*a*	2.793 (2)
Al6*a*—1Co3*a*	2.708 (2)	Si3*b*—1Co3*a*	2.294 (1)
Al6*a*—1Si3*b*	2.734 (2)	Si3*b*—1Co2*b*	2.317 (1)
Al6*a*—1Al3*b*	2.741 (1)	Si3*b*—1Si1*a*	2.505 (2)
Al6*a*—1Si3*a*	2.793 (2)	Si3*b*—1Al3*b*	2.550 (1)
Si3*a*—1Co3*b*	2.299 (1)	Si3*b*—1Si3*a*	2.583 (2)
Si3*a*—1Co2*a*	2.308 (1)	Si3*b*—1Al4*a*	2.588 (1)
Si3*a*—1Si1*a*	2.479 (2)	Si3*b*—1Al5*b*	2.705 (2)
Si3*a*—1Si3*b*	2.583 (2)	Si3*b*—1Al6*a*	2.734 (2)
Si3*a*—1Al4*b*	2.585 (2)	Si3*b*—1Al3*a*	2.843 (2)
Si3*a*—1Al3*a*	2.589 (1)		

† Occupancy 0.50.

The refined occupancy of 50% for the chain positions Si3 and Al6 agrees very well with the analysis of distances between these positions, showing that a reasonable model is only possible when every second site along the chain is empty (Fig. 3*a*). Si3 and Al6 in the subcell model are thus describing a superposition of different orientations of the chains and it is safe to assume that the superstructure reflections are a consequence of clear order in each (Si—Si—Al) chain. The Al6 position may be considered as the 'origin' of the chain. It can be located either at $y = \frac{1}{4}$ or $\frac{3}{4}$ (*Pnma* model). These four different orientations of the chain with respect to the planar layer are denoted as A, B, C and D (Fig. 3*b*).

Starting from the subcell model we tried to transfer an ordered variant of the substructure into a unit cell with doubling of both short axes, as indicated by oscillation photographs. The large unit cell [*C*-centered Bravais lattice; $a = 8.0839$ (3), $b = 14.5445$ (6), $c = 21.3536$ (9) Å] allowed the description of all strong and weak reflections observed on the collected images. Systematic extinctions revealed the diffraction symbol *C-c-* with *Cmcm*, $Cmc2_1$ and *Ama*2 as possible space groups. The structure motif in the non-centrosymmetric space group $Cmc2_1$ was developed from the subcell model and resulted in 35 independent atomic sites. The refinement resulted in a residual of $R_F = 0.033$ and a Flack parameter (Flack, 1983) of 0.44 (2), which indicated the presence of two inverse atomic arrangements in the investigated specimen

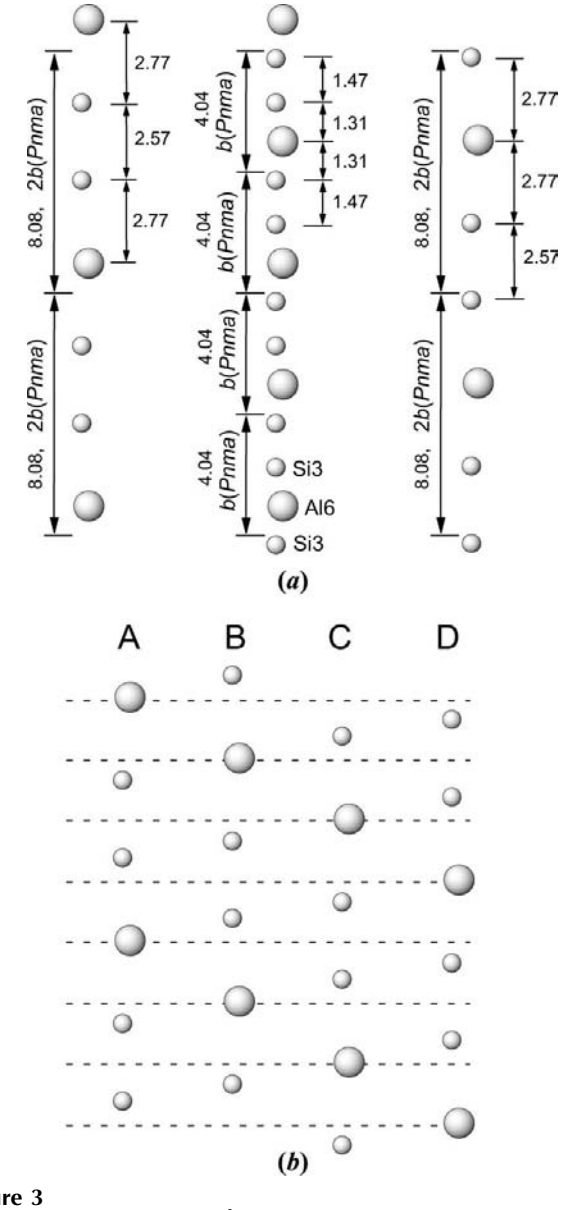

Figure 3
(*a*) Interatomic distances (in Å) between partially occupied (50%) atomic positions Al6 and Si3 in the *Pnma* model. (*b*) The possible relative arrangements of the Si and Al species within adjacent (Si—Si—Al) chains. Dashed lines symbolize planar layers.

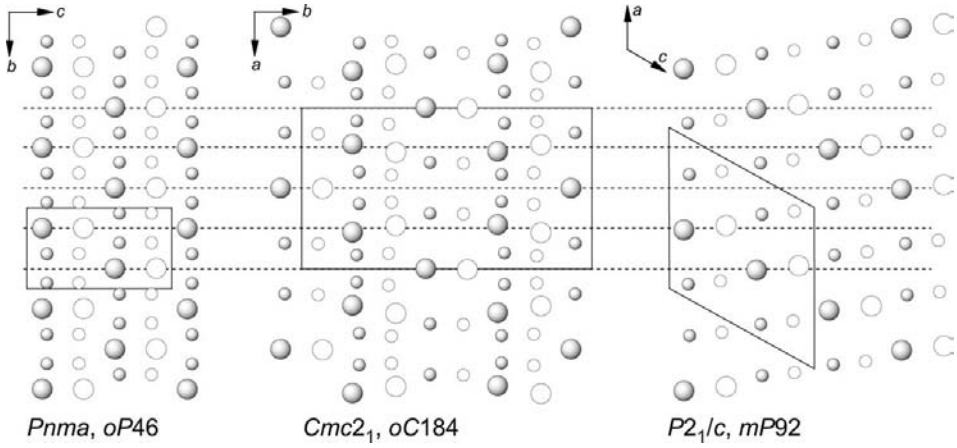

Figure 4
Relative arrangements of (Si—Si—Al) chains and planar layers in the different structural models for $Co_6Al_{11-x}Si_{6+x}$: view along the longest structural axis (21.35 Å). The planar layers are symbolized by dashed lines. Shaded atoms: front; open atoms: behind.

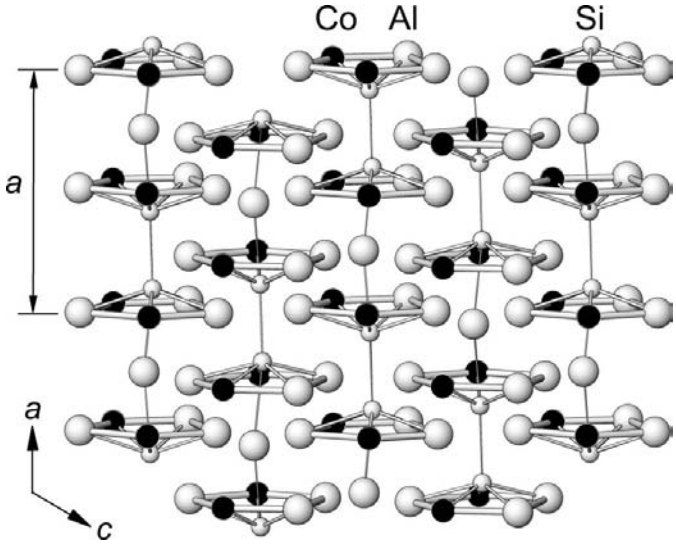

Figure 5
Interaction between the atoms of (Si—Si—Al) chains and the adjacent layers. The axes shown correspond to the monoclinic model.

(inversion twin). Atomic coordinates and displacement parameters for $Co_6Al_{11-x}Si_{6+x}$ in the space group $Cmc2_1$ are given as supplementary material.[2] Surprisingly, it is not possible to describe the chains in a totally ordered manner in $Cmc2_1$. While half of the chains (Si3*c*—Si3*c*—Al6*b*) are fully ordered within $Cmc2_1$, the other half (Si3*a*—Si3*b*—Al6*c*) have to be assigned with 50% occupancy. Thus, within the space group $Cmc2_1$ the latter chain may adopt two different orientations with respect to the layers. A view along the (long) *c* axis of the structural model showing the arrangement of chains is given in Fig. 4.

In order to clarify if it is possible to describe the whole structure with a completely ordered model, several attempts were made to refine the crystal structure in lower-symmetry space groups. An ordered structural model could finally be identified in a primitive monoclinic setting (space group $P2_1/c$, $a = 8.085$, $b = 21.373$, $c = 8.319$ Å, $\beta = 119.1°$), which can be obtained by the transformation of the orthorhombic *C*-centered unit cell using transformation matrix $(1\,0\,0, 0\,0\,\bar{1}, \frac{1}{2}\,\frac{1}{2}\,0)$. Refinement employing this model resulted in relatively high residuals of $R_F = 0.10$ and $wR_2 = 0.360$ and showed warning signs typical for merohedral twinning (Herbst-Irmer & Sheldrick, 1998): a set of reflections with systematic violation of the space-group symmetry was still present, $K = \text{mean}(F_o^2)/\text{mean}(F_c^2)$ was systematically high for reflections with low intensites, F_o for all 'most disagreeable' reflections were much greater than F_c *etc.* The refinement using the twin law $(1\,0\,0, 0\,1\,0, \bar{1}\,0\,\bar{1})$ significantly decreased the residuals to $R_F = 0.030$ and $wR_2 = 0.080$, and aligned all the mentioned inconsistencies. The refined ratio of twin components was found to be almost equal [0.521 (2):0.479 (2)]. Atomic and equivalent displacement parameters according to this model are given as supplementary material[3] and the respective projection of chains is shown in the right part of Fig. 4. The monoclinic structural model has a lower number of independent atomic sites (23 compared with 35 in the case of the $Cmc2_1$ model) and does not require half-filled positions in the (Si—Si—Al) chains.

The interatomic contacts determining the interactions between the chains and the layer are shown in Fig. 5. The position of the chains is determined by close contacts of the Si atoms belonging to the chains with two Co and three Al atoms within the next layer. No close contacts are formed to the other, more distant, net. Within a single chain the Si atoms are alternately orientated in conjunction yielding a Si—Si distance of approximately 2.57 Å or they are separated by an Al atom situated within the flat net. The Al—Si distance in the chain is approximately 2.75 Å.

The zigzag motifs formed by the chains (see also Fig. 2) are shown in Fig. 6 for the different structure models. In the $P2_1/c$ model (Fig. 6, right) all chains are ordered and described by a set of fully occupied positions (Si3*a*, Si3*b* and Al6*a*), yielding the sequence A–B–C–D within the zigzag motifs. In the $Cmc2_1$ model (Fig. 6, center) half of the chains are ordered (Al6*b* and Si3*c*), while the other half are disordered (50% occupied; Al6*c*, Si3*a*, Si3). The respective arrangements are repeated according to the *C*-centering of the unit cell yielding the sequence A–B/D–C–B/D within the zigzag motif. In the *Pnma*

[2] For details see supplementary Table 2.

[3] For details see supplementary Table 3.

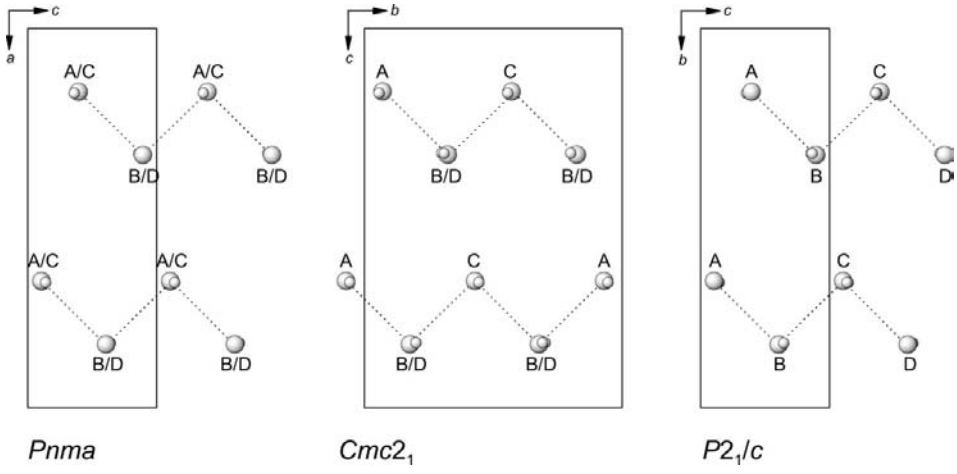

Figure 6
Relative arrangements of (Si—Si—Al) chains according to different structural models projected on the layers. The zigzag motifs and relative orientations according to Fig. 3 are shown. For better illustration the atoms located outside the chains are not shown.

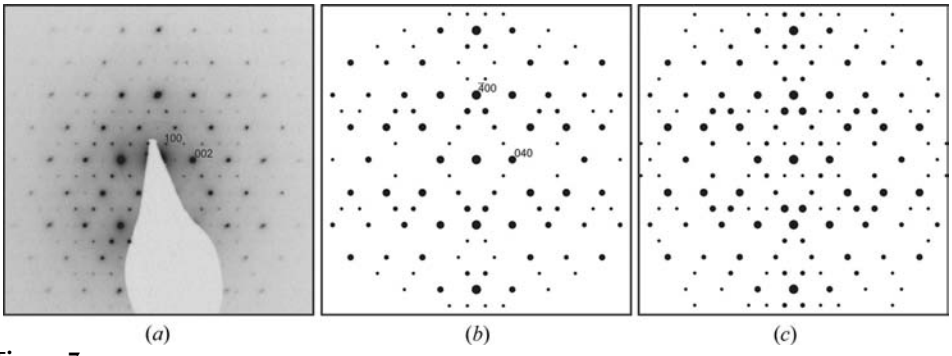

Figure 7
(*a*) Experimental SAED pattern for the [010] zone (axis notation of the $P2_1/c$ model); (*b*) simulated kinematical ED pattern for the [001] zone axis of the $Cmc2_1$ model; (*c*) simulated kinematical ED pattern for the [010] zone axis of the twinned $P2_1/c$ model with a twin domains ratio of 1:1.

model (Fig. 6, left) all chains are disordered and the relative positions A/C and B/D are alternately arranged.

The reasons for doubling in the [001] direction in the *Pnma* model [c(*Pnma*) = 7.2723 (3), b($Cmc2_1$) = 14.5445 (6) Å] may be rationalized with the help of Figs. 4 and 6. Local atomic arrangements around the penetration points within the layers control the orientation of the next chain with respect to the previous one. So the chain orientation A has to be followed either by B or by D. Thus, within the zigzag motif, only the two inverted sequences (. . . A–B–C–D . . .) or (. . . A–D–C–B . . .) are possible, but all four orientations A, B, C and D have to be present in the symmetrically independent part of the zigzag motif. This leads to the doubling of the cell parameters in both $Cmc2_1$ and $P2_1/c$ structural models.

For the successful refinement of the $Cmc2_1$ model, a Flack parameter of ~ 0.5 was necessary (inversion twin). The $P2_1/c$ model, on the other hand, required the refinement as a meroheral twin in the domain ratio 1:1. From the experimental point of view, however, we do not find any additional independent information that would justify regarding the observed crystals of $Co_6Al_{11-x}Si_{6+x}$ as twins, *i.e.* the detailed analysis of the metallographic sample under polarized light (Fig. 1) did not reveal any sign of twinning. Furthermore, analysis of the powder pattern in the high diffraction-angle region as well as the single-crystal X-ray data did not give any hint of a possible monoclinic distortion of the orthorhombic unit cell, as would be expected for the $P2_1/c$ model. A comparison of the experimental powder pattern[4] with the calculated patterns based on the two different models did not prefer one of the two models.

The ordered micro-twinning may occur at a scale that cannot be resolved by light microscopy. In order to check this possibility, a TEM investigation was performed. Selected-area electron diffraction (SAED) patterns were registered in various crystal orientations: [100], [010], [001], [102], [112], [302] (axis notation of the $P2_1/c$ model).

Agreement between experimental SAED patterns (area of 250 nm in diameter) simulated on the basis of the $P2_1/c$ model is generally poor. There seems to be a doubling of the unit cell along [010] or, at least, the violation of the general reflection condition $0k0$: $k = 2n$. Moreover, additional reflections can be noticed in the [100] orientation. These additional reflections do not fit the reciprocal lattice of the $P2_1/c$ model.

The SAED pattern at the [010] zone axis (Fig. 7*a*) approximately resembles the simulated pattern for the $Cmc2_1$ model (Fig. 7*b*), but also the twinned $P2_1/c$ model (Fig. 7*c*) with the twin domain ratio 1:1. There are, however, no twin domains observed in the corresponding TEM images (not shown here). In case twinning would be a reality, this could only be explained assuming the twin intergrowth zones are perfectly planar and parallel to (010), so that the twin individuals would alternate along [010] with a volume ratio of 1:1. This rather unlikely scenario is clearly eliminated by the SAED patterns and high-resolution TEM images for the directions orthogonal to [010] of the $P2_1/c$ model, which also do not reveal twin domains.

The fact that the SAED pattern resembles the twin models without showing twin domains even at this level of reso-

[4] See supplementary material (powder diffraction file in CIF format).

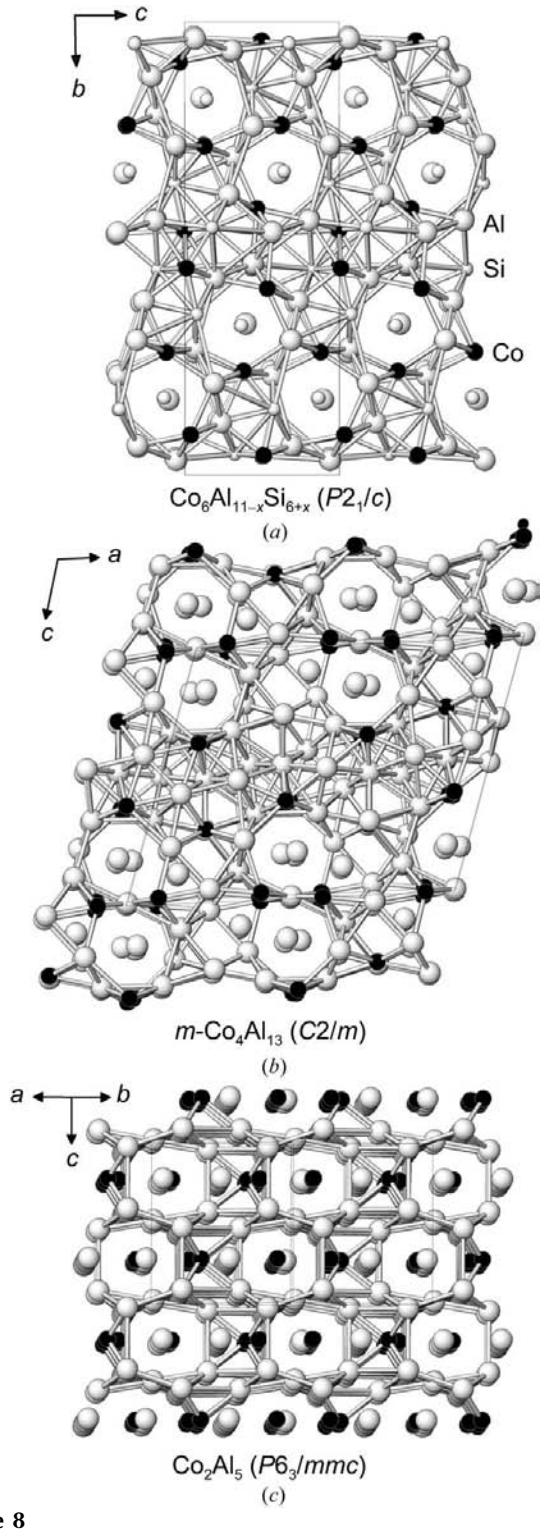

Figure 8
Pentagonal antiprismatic channels as the common structural motif for some aluminium-rich compounds: (*a*) $Co_6Al_{11-x}Si_{6+x}$: projection along [100]; (*b*) m-Co_4Al_{13}: projection along [010]; (*c*) Co_2Al_5: projection along [110]. The bonds between the atoms of the axis of the channels and the atoms of the channel walls are omitted for clarity.

lution may be interpreted as follows. In contrast to the (. . . A–B–C–D . . .) ordering within the zigzag motifs, there is no structural reason for the full alignment of the two adjacent

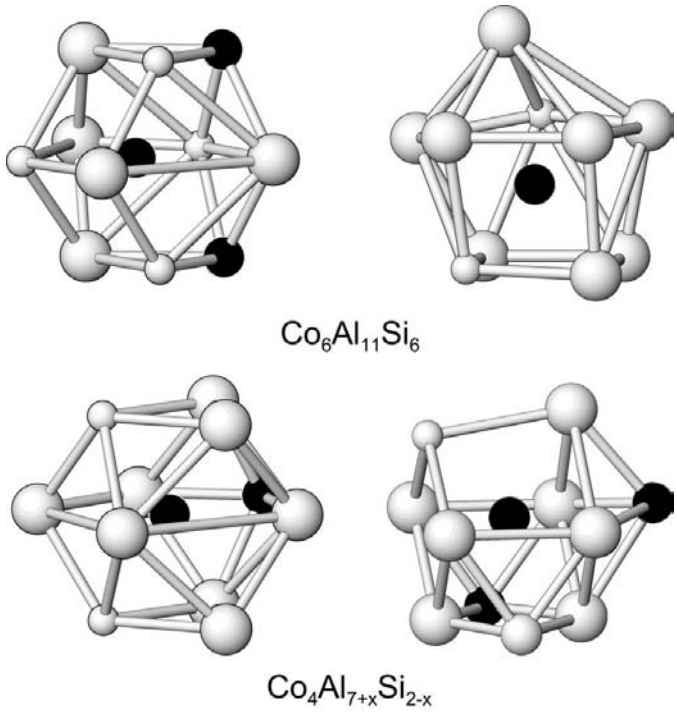

Figure 9
Comparison of the coordination environments of the Co atoms in $Co_6Al_{11-x}Si_{6+x}$ and $Co_4Al_{7+x}Si_{2-x}$.

zigzag motifs as the distance between them is of the order 10 Å (Fig. 7*c*). The disorder between adjacent zigzag motifs cannot be completely described by the symmetry of the appropriate space groups and requires introducing the merohedral twin law in a 1:1 ratio to the ordered $P2_1/c$ model or inverse twins for the $Cmc2_1$ model for a complete description of the experimental diffraction data.

The structural relations of $Co_6Al_{11-x}Si_{6+x}$ to the adjacent binary cobalt aluminides and related compounds can be seen in Fig. 8. A common structural feature of the binary phases Co_2Al_5 and the phase bundle around the Co_4Al_{13} composition which consists of the three phases o-Co_4Al_{13} ($oP102$, $Pmn2_1$, own structure type; Grin *et al.*, 1994*a*), m-Co_4Al_{13} ($mC102-7.2$, Cm, own structure type; Hudd & Taylor, 1962; Burkhardt *et al.*, 1996) and h-Co_4Al_{13} ($mC34$, $C2/m$, structure type Os_4Al_{13}; Gödecke & Ellner, 1996) is the occurrence of 'channels' or columns formed by condensed pentagonal prisms which are centered by Co and Al atoms. These channels are structural motifs which are helpful for the visualization of the crystal structures. It should be pointed out, however, that chemical interactions between atoms situated within the channels and those surrounding the channels do not differ at all. Thus, the term 'channel' refers to a visualization concept rather than to a bonding feature. The channels are condensed to pairs or form more complex arrangements within the respective unit cell (Burkhardt *et al.*, 1996). A similar structural motif was observed in a number of transition-metal aluminides and gallides like V_2Ga_5, Fe_2Al_5, V_7Al_{45}, V_4Al_{23} and VAl_{10} (Grin *et al.*, 1994*b*). In the compound

$Co_6Al_{11-x}Si_{6+x}$ pentagonal prismatic channels form the surrounding of the (Si—Si—Al) chains discussed above and are interconnected to a zigzag arrangement. The level of channel interconnection is lower than in *m*-Co_4Al_{13} (Fig. 8, middle) and Al_5Co_2 (Fig. 8, bottom).

In contrast to $Co_6Al_{11-x}Si_{6+x}$ the neighboring ternary χ phase, $Co_4Al_{7+x}Si_{2-x}$ reported recently (Richter *et al.*, 2005) does not show the pentagonal channel motif, because no icosahedral or pentagonal prismatic coordination for any of the Co or Al (Si) sites is present in the crystal structure of $Co_4Al_{7+x}Si_{2-x}$. Instead, the coordination of the Co atoms (trigonal prisms with five additional vertices) was identified as the common structural feature present in $Co_4Al_{7+x}Si_{2-x}$ as well as in chemically related binary and ternary aluminides. A 'cluster' formed by two trigonal prisms around cobalt (transition metal) and a distorted rectangular prism around the aluminium was identified as the common structural motif in the crystal structures of $Co_4Al_{7+x}Si_{2-x}$, *o*-Co_4Al_{13} and Fe_4Al_{13} (Richter *et al.*, 2005). These 'clusters' are not present in $Co_6Al_{11-x}Si_{6+x}$, but the coordination environment of the Co atoms found in $Co_6Al_{11-x}Si_{6+x}$ as well as in $Co_4Al_{7+x}Si_{2-x}$ is very similar (Fig. 9), which emphasizes the close chemical relationship of these compounds. The coordination environments of Co1 (left, top) and Co2 (right, top) in $Co_6Al_{11-x}Si_{6+x}$ closely resemble the coordinations of Co1 (left, bottom) and Co2 (right, bottom) found in $Co_4Al_{7+x}Si_{2-x}$.

One of the most striking features of the crystal structure of $Co_6Al_{11-x}Si_{6+x}$ is the existence of very short Co—Si distances. A list of selected interatomic distances given in Table 3 reveals that each Co atom shows two very close contacts to adjacent Si atoms. The respective distances are 2.22–2.30 Å, *i.e.* small compared with the usual interatomic Co—Si distances in binary compounds such as $CoSi_2$ (CaF_2-type, *cF*12) and Co_2Si (own structure type, *oP*12; Villars & Calvert, 1991) showing Co—Si distances of at least 2.32 Å. The short Co—Si distances favor the clear separation of Si and Al positions in $Co_6Al_{11-x}Si_{6+x}$ as a substitution of Si by Al is not possible in any case. As a consequence, $Co_6Al_{11-x}Si_{6+x}$ shows a very narrow composition range and no mixed occupation of the Si positions. On the other hand, limited substitution of Si at Al sites appears to be present in this compound, as reflected by the small but noticeable deviation of the composition determined by EPMA ($Co_{26.4}Al_{44.4-46.6}Si_{29.2-27.0}$) from the chemical composition $Co_6Al_{11}Si_6$ ($Co_{26.1}Al_{47.8}Si_{26.1}$) derived from the crystal structure determination.

Comparing the interatomic distances detected between Co and Si/Al with the sum of the covalent radii $r_{Co} = 1.16$, $r_{Si} = 1.17$ and $r_{Al} = 1.25$ Å (Emsley, 1994), strong Co—Si and Co—Al bonding would be assumed in this compound. In terms of the Pauling bond order (Pauling, 1948), which depends solely on the interatomic distances, the short Co—Si distances observed in the ε phase (2.22–2.30 Å) would correspond to bond orders between 1.5 and 1.1 (*i.e.* strong bonding). The same is true for the closest Co—Al distances, which also correspond to bond orders around 1.

The calculation of the electron localization function (ELF) performed on the compound $Co_4Al_{7+x}Si_{2-x}$ (χ phase) reported recently (Richter *et al.*, 2005), however, yields a different picture of the chemical bonding in Al-rich Co–Al–Si compounds: in spite of very short Co—Si and Co—Al interatomic distances, no covalent interactions between Co and Al or Si was observed. In contrast, the signatures for directed (covalent) bonding were only found to be within the Al—Al and Al—Si contacts. The bonding situation in $Co_4Al_{7+x}Si_{2-x}$ corresponds to a covalently bonded network of Al and Si atoms, while the interactions between Co and the network are rather ionic in nature. Although it was not possible to perform a similar calculation for the ε phase, due to the large unit cell, we conclude that the principal bonding situation in the ε phase is probably comparable to the bonding observed for the χ phase which is reflected by the similarities observed in the Co coordination (see Fig. 9).

4. Conclusions

$Co_6Al_{11-x}Si_{6+x}$ adopts a crystal structure which is characterized by planar layers forming the main part of the structure. These layers can be described completely by an orthorhombic subcell model (*oP*46, space group *Pnma*). The observed doubling of two axes of the orthorhombic subcell is due to the ordering within and between penetrating (Si—Si—Al) chains. This ordering can be partially described either with an orthorhombic *C*-centered structure model (*oC*184, space group $Cmc2_1$), refined as inverse twins, or with an alternative monoclinic structure model (Pearson symbol *mP*92, space group $P2_1/c$), refined as a merohedral twin. However, we have observed neither signs of a monoclinic distortion in the diffraction patterns nor any other experimental evidence for twinning. Additional TEM studies did not confirm a complete order even within a very small domain size. Obviously, the interchain disorder is an inevitable feature of this structure. A completely ordered arrangement of (Si—Si—Al) chains within zigzag motifs is combined with an arbitrary arrangement of adjacent zigzag motifs.

Financial support from the Austrian Science Foundation (FWF) under the project numbers P14762-PHY and P19305-N19 is gratefully acknowledged. KWR would also like to thank the Max-Planck Society for research fellowship. The authors acknowledge gratefully U. Burkhardt and K. Schulze for their assistance in metallography and EDXS, respectively.

References

Akselrud, L. G., Zavalii, P. Y., Grin, Yu. N., Pecharsky, V. K., Baumgartner, B. & Wölfel, E. (1993). *Mater. Sci. Forum*, **133–136**, 335–340.

Boström, M., Rosner, H., Burkhardt, U., Prots, Yu. & Grin, Yu. (2005). *Z. Anorg. Allg. Chem.* **631**, 534–541.

Bruker Analytical X-ray Instruments Inc. (1997). *XPREP*, Version 5.1. Bruker Analytical X-ray Instruments Inc., Madison, Wisconsin, USA.

Burkhardt, U., Ellner, M. & Grin, Yu. (1996). *Powder Diffr.* **11**, 123–128.

Burkhardt, U., Ellner, M., Grin, Yu. & Baumgartner, B. (1998). *Powder Diffr.* **13**, 159–162.

Douglas, A. M. B. (1950). *Acta Cryst.* **3**, 19–24.
Emsley, J. (1994). *The Elements.* Berlin: Walter de Gruyter.
Flack, H. D. (1983). *Acta Cryst.* A**39**, 876–881.
Gödecke, T. & Ellner, M. (1996). *Z. Metallkd.* **87**, 854–864.
Grin, Yu., Burkhardt, U., Ellner, M. & Peters, K. (1994*a*). *J. Alloys Compd.* **206**, 243–247.
Grin, Yu., Burkhardt, U., Ellner, M. & Peters, K. (1994*b*). *Z. Kristallogr.* **209**, 479–487.
Grushko, B., Wittenberg, R., Bickmann, K. & Freiburg, C. (1996). *J. Alloys Compd.* **233**, 279–287.
Herbst-Irmer, R. & Sheldrick, G. M. (1998). *Acta Cryst.* B**54**, 443–449.
Herman, N. V. (1981). *Visnyk L'viv. University Ser. Chim.* **23**, 61–64.
Hudd, R. C. & Taylor, W. H. (1962). *Acta Cryst.* **15**, 441–442.
Li, X. Z. & Hiraga, K. J. (1998). *J. Alloys Compd.* **269**, L13–L16.
Ma, X. L. & Kuo, K. H. (1992) *Metall. Trans. A*, **23**, 1121–1128.
Pauling, L. (1948). *The Nature of the Chemical Bond.* New York: Cornell University Press.
Richter, K. W. (2002). *J. Alloys Compd.* **338**, 43–50.
Richter, K. W., Chandrasekaran, K. & Ipser, H. (2004). *Intermetallics*, **12**, 545–554.
Richter, K. W. & Prots, Yu. (2006*a*). *Z. Kristallogr. New Cryst. Struct.* **221**, 112−114.
Richter, K.W. & Prots, Yu. (2006*b*). *Z. Kristallogr. New Cryst. Struct.* **221**, 115–118.
Richter, K. W., Prots, Yu. & Grin, Yu. (2004). *Z. Anorg. Allg. Chem.* **630**, 417–422.
Richter, K. W., Prots, Yu. & Grin, Yu. (2005). *Inorg. Chem.* **44**, 4576–4585.
Richter, K. W. & Tordesillas Gutiérrez, D. (2005). *Intermetallics*, **13**, 848–856.
Sheldrick, G. M. (1997). *SHELX*97. University of Göttingen, Germany.
Villars, P. & Calvert, L. D. (1991). Editors. *Pearson's Handbook of Crystallographic Data*, 2nd Ed. Ohio: ASM International.